Purification of Rift Valley Fever Virus-Like Particles for Structural Analyses

MASTER'S THESIS

Liina Hannula
UNIVERSITY OF HELSINKI | MASTER'S PROGRAMME IN MICROBIOLOGY AND MICROBIAL BIOTECHNOLOGY

HELSINGIN YLIOPISTO
HELSINGFORS UNIVERSITET
UNIVERSITY OF HELSINKI

Tiedekunta – Fakultet – Faculty	Koulutusohjelma – Utbildningsprogram – Degree Programme
Faculty of Acriculture and Forestry ¤ And Faculty of Biological and Environmental Sciences ¤coordinating faculty	Master's Programme in Microbiology and Microbial Biotechnology

Tekijä – Författare – Author
Liina Hannula

Työn nimi – Arbetets titel – Title
Purification of Rift Valley Fever Virus-Like Particles for Structural Analyses

Oppiaine/Opintosuunta – Läroämne/Studieinriktning – Subject/Study track
Virology

Työn laji – Arbetets art – Level	Aika – Datum – Month and year	Sivumäärä – Sidoantal – Number of pages
Master's thesis	5/2020	35

Tiivistelmä – Referat – Abstract

Rift Valley fever virus (RVFV) is a mosquito-borne virus of the order Bunyavirales with a tripartite (-)ssRNA genome. It infects humans and cattle, causing a febrile disease with symptoms ranging from mild to severe. Safe and efficient human vaccines have not yet been developed, which underlines the importance of gaining a clear understanding of the viral antigenic surface.

One significant challenge for RVFV research is posed by the costly and time-consuming biosafety precautions warranted by the pathogenicity of the virus. The surface of RVFV, formed by the two viral envelope glycoproteins Gn and Gc, could also be studied with a non-pathogenic model, such as a virus-like particle (VLP). A VLP is a macromolecular complex that resembles the virus, especially with respect to its outer structure, but lacks the viral genome.

In this work, RVFV VLPs were produced by transient transfection of mammalian cells with genes encoding RVFV glycoproteins Gn and Gc . The objective was to design an optimized production and purification pipeline for RVFV VLPs to elucidate their structure by cryo-electron microscopy. To optimize the VLP production and purification, the effect of sample harvest times and DNA-to-cell ratios of transfection on RVFV glycoprotein expression was examined. Several methods were tested for VLP sample concentration and purification. VLPs were successfully detected in the purified samples by immuno-electron microscopy.

Despite some challenges related to sample purity and scarcity of VLPs in samples, which prevented analyses by cryo-electron microscopy, the expression system described in this thesis has great potential to streamline RVFV VLP sample preparation for electron microscopy and to accelerate vital research into the structural properties of this emerging pathogen.

Avainsanat – Nyckelord – Keywords
Rift Valley Fever Virus, virus-like particle, *Bunyavirales*, structural biology, biocomplex purification

Ohjaaja tai ohjaajat – Handledare – Supervisor or supervisors
Juha Huiskonen and Elina Roine

Säilytyspaikka – Förvaringsställe – Where deposited
HELDA - Helsingin yliopiston digitaalinen arkisto / HELDA - Helsingfors universitets digitala publikationsarkiv /HELDA - Digital Repository of the University of Helsinki

Muita tietoja – Övriga uppgifter – Additional information

HELSINGIN YLIOPISTO
HELSINGFORS UNIVERSITET
UNIVERSITY OF HELSINKI

Tiedekunta – Fakultet – Faculty	Koulutusohjelma – Utbildningsprogram – Degree Programme
Maa- ja metsätaloustieteellinen tiedekunta ¤ Ja Bio- ja ympäristötieteellinen tiedekunta ¤koordinoiva tiedekunta	Mikrobiologian ja mikrobibiotekniikan maisteriohjelma

Tekijä – Författare – Author
Liina Hannula

Työn nimi – Arbetets titel – Title
Rift Valley Fever -viruksen kaltaisten partikkelien puhdistus rakenteellisia analyysejä varten

Oppiaine/Opintosuunta – Läroämne/Studieinriktning – Subject/Study track
Virologia

Työn laji – Arbetets art – Level	Aika – Datum – Month and year	Sivumäärä – Sidoantal – Number of pages
Maisterintutkielma	5/2020	35

Tiivistelmä – Referat – Abstract

Rift Valley Fever -virus (RVFV) on hyttyslevitteinen (-)ssRNA-virus (lahko *Bunyavirales*), jonka genomi koostuu kolmesta RNA-segmentistä. RVFV aiheuttaa ihmisissä ja karjaeläimissä vakavuudeltaan vaihtelevaa kuumetautia. Turvallisia ja tehokkaita ihmisrokotteita ei ole vielä kehitetty, mikä korostaa viruksen ja isännän vuorovaikutuksen sekä viruspartikkelin immunogeenisen pinnan tuntemisen tärkeyttä.

RVFV:n taudinaiheuttamiskyky tekee sen tutkimisesta haastavaa, sillä viruksen käsittely edellyttää bioturvallisuusjärjestelyjä, jotka ovat usein kalliita ja aikaa vieviä. RVFV:n ulkopinnan rakennetta, joka koostuu viruksen Gn- ja Gc-glykoproteiineista, on myös mahdollista tutkia käyttämällä vaaratonta mallia, kuten viruksen kaltaista partikkelia (VLP). VLP on makromolekulaarinen kompleksi, joka muistuttaa virusta etenkin ulkokuorensa osalta, mutta ei sisällä sen perimää.

Tässä työssä RVFV-viruksen kaltaisia partikkeleita tuotettiin viemällä nisäkässoluihin RVFV:n Gn- ja Gc-glykoproteiineja koodaavat geenit. Tavoitteena oli suunnitella tehokas protokolla Rift Valley Fever -viruksen kaltaisten partikkelien tuottoon ja puhdistukseen niiden rakenteen tutkimiseksi kryoelektronimikroskopian avulla. VLP:iden tuoton optimoimiseksi VLP-näytteiden keruuaikojen sekä nisäkässoluihin viedyn DNA-määrän vaikutuksia tuottoon testattiin. VLP:iden konsentroinissa ja puhdistuksessa vertailtiin useita eri menetelmiä. VLP:itä havaittiin onnistuneesti immunoelektronimikroskopian avulla.

Näytteiden puhtaus sekä VLP:iden harvalukuisuus näytteissä ovat toistaiseksi estäneet tarkemmat kryoelektronimikroskopia-analyysit. Tässä työssä kuvatuilla tuottomenetelmillä on kuitenkin potentiaalia yksinkertaistaa VLP-näytteiden tuottoa elektronimikroskopiaa varten, mikä edistäisi elintärkeää tutkimusta tämän uhkaavan taudinaiheuttajan rakenteellisista ominaisuuksista.

Avainsanat – Nyckelord – Keywords
Rift Valley Fever -virus, viruksen kaltainen partikkeli, *Bunyavirales*, rakennebiologia

Ohjaaja tai ohjaajat – Handledare – Supervisor or supervisors
Juha Huiskonen ja Elina Roine

Säilytyspaikka – Förvaringsställe – Where deposited
HELDA - Helsingin yliopiston digitaalinen arkisto / HELDA - Helsingfors universitets digitala publikationsarkiv /HELDA - Digital Repository of the University of Helsinki

Muita tietoja – Övriga uppgifter – Additional information

1 TABLE OF CONTENTS

2 ABBREVIATIONS

Cryo-EM = cryo-electron microscopy / electron cryo-microscopy

CsCl = cesium chloride

DMEM = Dulbecco's modified Eagle's medium

EM = electron microscopy

EV = extracellular vesicle

kDa = kilodalton

MWCO = molecular weight cutoff

NMCO = nominal molecular weight cutoff

PEG = polyethylene glycol

PEI = polyethyleneimine

PFA = paraformaldehyde

RVFV = Rift Valley fever virus

TEM = transmission electron microscopy

VLP = virus-like particle

Å = angstrom

3 INTRODUCTION

Rift Valley fever virus (RVFV) is the causative agent of a mosquito-borne zoonosis that affects humans and livestock. The symptoms range from mild and flu-like to a more severe hemorrhagic fever with neurological complications (Wright et al., 2019). RVFV was originally isolated in East Africa, but epidemics and epizootics have since been observed in Northern Africa and the Arabic Peninsula (Kortekaas, 2014). Factors including climate change and wide distribution of suitable mosquito vectors warrant concerns about RVFV spreading on the global scale (Paweska & van Vuren, 2013). Currently, there is no safe and efficient licensed vaccine against RVFV for humans, though several veterinary vaccines are in use in the affected areas (WHO, 2018). RVFV poses a significant threat to human and animal health, making the development of vaccines and treatments a priority.

RVFV is a single-stranded RNA virus that belongs to the order *Bunyavirales*, family *Phenuiviridae*, and genus *Phlebovirus* (Abudurexiti et al., 2019). The RVFV lipid envelope encapsulates the three RNA segments of the genome that form a ribonucleoprotein complex together with a viral nucleoprotein (Figure 1; Michele Bouloy & Weber, 2010). The medium (M) segment of the genome encodes the two glycoproteins, Gn and Gc, embedded in the viral envelope (Spiegel et al., 2016). Gn and Gc assemble into heterodimers, which in turn form the hexamers and pentamers that constitute the viral surface with its ring-shaped structures characteristic to RVFV (Halldorsson et al., 2018; Huiskonen et al., 2009).

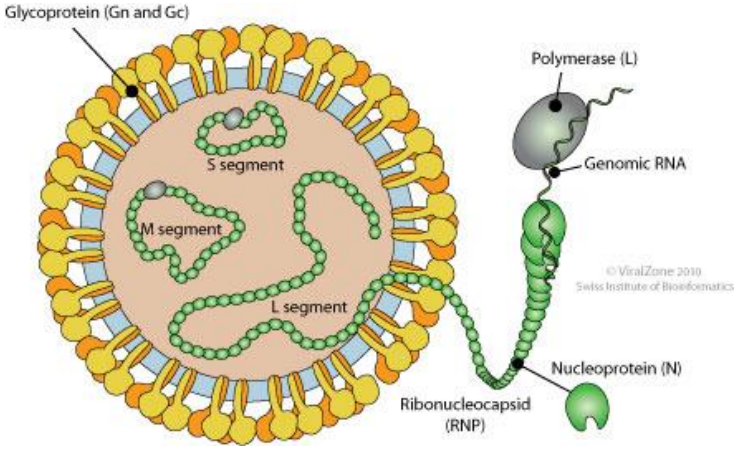

Figure 1. Overview of the structure of the RVFV virion. *Genomic segments of RVFV (L, M, and S), nucleoprotein, viral RNA-dependent RNA polymerase, and glycoproteins are indicated. Image acquired from SIB Swiss Institute of Bioinformatics: ViralZone.*

RVFV glycoproteins play a central role in several stages of the infection process. RVFV virions are taken up into host cells by caveolin– mediated endocytosis (Harmon et al., 2012), which is catalyzed by RVFV glycoproteins interacting with receptors on the host cell surface, most importantly the C-type lectin DC-SIGN (Lozach et al., 2011). Escape from late endosomes is triggered by low pH, which leads to conformational changes in the glycoproteins. The fusion loop of Gc, a class II fusion protein, is revealed and inserted into the endosomal membrane, catalyzing the fusion of viral and host membranes (Halldorsson et al., 2018). The RVFV glycoprotein shell is also a key target for neutralizing antibodies (Faburay et al., 2017) and prospective antivirals (Atkins & Freiberg, 2017), which emphasizes the importance of resolving RVFV structure to near-atomic level to facilitate the design of vaccines and antiviral measures.

A detailed reconstruction of the surface structure of the virion was recently obtained by cryo-electron microscopy (cryo-EM). Due to the innate flexibility of RVFV envelope proteins, the resolution of the reconstruction was limited to 7.7 Å, despite application of novel computational analysis techniques (Halldorsson et al., 2018). The study of the outer structure of RVFV is additionally complicated by the biosafety prerequisites for handling the pathogenic virus. Conducting structural biology work in biosafety level 3 facilities is often time-consuming and costly (Sherman et al., 2013). Developing models to represent the native conformation of the surface of RVFV would help circumvent this challenge.

A non-infectious virus-like particle (VLP) that lacks the viral genome but displays the native outer structure of RVFV has great potential as a model in structural studies. VLPs can be produced by using host cells to express selected viral genes, that encode structural protein components of the virus (Zeltins, 2013). The formation of RVFV VLPs in host cells has been implicated to require the expression of the viral nucleoprotein, in addition to envelope glycoproteins (Habjan et al., 2009). Other evidence suggests that RVFV VLPs can be released in the absence of the nucleoprotein, only less efficiently than virions or nucleoprotein-including VLPs (Piper et al., 2011). Indeed, VLPs based solely on heterologous expression of the two glycoproteins Gn and Gc have been successfully produced and imaged by transmission

electron microscopy (Mandell et al., 2010a). The particles seem to resemble RVFV virions in size and morphology, but a more in-depth structural analysis is warranted.

The objective of this work was to assess whether RVFV VLPs, formed by expression of RVFV Gn and Gc in mammalian cells, could be used for modelling the outer structure of RVFV. In earlier studies, RVFV VLPs have been successfully expressed in various platforms, including insect cells (Li et al., 2016; Mandell et al., 2010b), suspension-adapted mammalian cells (Mandell et al., 2010b), and adherent mammalian cells (Habjan et al., 2009; Mandell et al., 2010a). Here, we set up a VLP expression system by transiently transfecting adherent HEK293T cell cultures with a pLEXm-derived plasmid (Aricescu et al., 2006) encoding RVFV glycoproteins. Importantly, the process of VLP production and purification was analyzed and optimized with the aim of producing high-quality VLP samples for cryo-EM. Reconstructions based on cryo-EM data can be used to gain insights on the ultrastructure of the VLPs, and thus to assess the resemblance of VLPs to RVFV virions. If proving to sufficiently resemble the virions, VLPs have great promise for accelerating research on the structure and function of RVFV and related viruses.

4 MATERIALS & METHODS

4.1 REAGENTS AND CULTURING MEDIA

Bacterial cultures were maintained in LB broth or on LB agar (for formulation, see Tables S1 and S2), supplemented with 100 µg/ml ampicillin. DMEM (for formulation, see Table S3) was used as the mammalian cell culturing medium. Unless otherwise mentioned, DMEM was supplemented with 10% FBS (Gibco), MEM non-essential amino acid solution (each amino acid at 0.1 mM concentration; Gibco) and 2 mM L-glutamine (Gibco). Trypsin-(0.05%)-EDTA solution was used to detach the cells (for formulation, see Table S4).

The primary antibody used for all immunodetection of RVFV Gn glycoprotein was monoclonal rabbit anti-RVFV Gn (300 µg/ml) (Allen et al., 2018), that recognizes the native conformation of RVFV Gn. HRP-conjugated anti-rabbit monoclonal antibody GOXRB HRP XADS (1 mg/ml; Novex) was used as the secondary antibody in dot blots.

For immunogold labeling of electron microscopy grids, 15 nm gold-conjugated goat anti-rabbit IgG (BBI International) was used, diluted to a working concentration of 2.04 µg/ml.

4.2 PLASMIDS, CELLS, AND CULTURE GROWTH CONDITIONS

Escherichia coli DH5α was used as the host for plasmid propagation. Plasmid-carrying cultures were grown at +37 °C with shaking. The Gn/Gc-expression plasmid for VLP expression was constructed using pHLsec, a pLEXm-derived mammalian expression plasmid, as a backbone (Aricescu et al., 2006). It includes an ampicillin resistance gene and a gene encoding a fluorescent mTurquoise tag (Goedhart et al., 2010). The plasmid pKSII (Stratagene) was used as a negative control plasmid for transfection.

HEK293T human embryonic kidney cells were grown as adherent cultures at +37 °C with humidification and a 5 % CO_2 atmosphere. Total volume of culturing medium was 25 ml in 175 cm^2 flasks and 10 ml in 75 cm^2 flasks. Cells were split 1:10 to 1:5 at 80–90% confluence, with 3–4-day intervals. To split the cells, culturing medium was removed, after which the cells were gently rinsed with 1 × PBS and detached using 3–5 ml trypsin-EDTA. The detached cells were resuspended by adding 10 ml culturing medium, and excess trypsin was removed by centrifuging the cells (300 × g, 5 minutes, +20 °C) and removing the supernatant. The cell pellet was resuspended in 10 ml of culture medium, after which cell count of the suspension was determined and a suitable volume was pipetted into a flask with fresh medium to start the new culture.

The cell density of the resuspension was determined with TC20 cell counter (Bio-Rad). A 10 µl aliquot of a 1:1 mixture of trypan blue solution and cell suspension was pipetted in a chamber of a cell counting slide. All cell counts reported here are averages of at least two parallel cell counts.

Frozen cell stocks were stored in a mechanical freezer at – 75 °C. The stocks were prepared from fresh cultures at approximately 90% confluence. To prepare a stock, the cells were washed with 25 mL PBS, and detached using 3 mL trypsin-EDTA. 10 mL culture medium was added to the detached cells, and the suspension was centrifuged at 300 × g for 5 minutes. The cell pellet was resuspended in 5 mL freezing medium (DMEM with 20% FBS, 10% DMSO) and aliquoted into 1 mL cryotubes. The stocks

were frozen by storing them in a cell freezing apparatus (Mr. Frosty™, ThermoFisher Scientific) with isopropanol at −75 °C, for 5.5 hours to overnight, after which they were transferred to a regular container at the −75 °C freezer.

A new culture was started from a frozen cell stock by thawing it rapidly at +37 °C and pipetted into 5 ml fresh culturing medium. The cell suspension was centrifuged at 300 × g, +20 °C, for 3 minutes, to remove DMSO from cells. The cell pellet was resuspended into 6 ml fresh culturing medium and transferred into a 25 cm^2 flask for incubation.

4.3 CLONING AND PLASMID PURIFICATION

The Gn/Gc-expression plasmid had been constructed prior to this thesis work by ligating a synthetic cDNA fragment corresponding to the RVFV clone 13 M segment region encoding Gn and Gc into the plasmid backbone. A tag-free version of the Gn/Gc-expression plasmid with the same components excluding the mTurquoise gene had also been constructed. The correct composition of the plasmids had been confirmed by sequencing.

Plasmids were extracted from 2 L bacterial cultures grown for 18–22 h using EndoFree Plasmid Mega Kit (Qiagen), according to the manufacturer's instructions. The DNA concentration of the plasmid preparation was measured with BioPhotometer (Eppendorf). Aliquots of the DNA sample being measured were diluted with elution buffer as needed for the A_{260} value to be in the range for reliable measurements (0.1–1).

The plasmid pKSII (Stratagene) was used as a negative control plasmid for transfection. It was propagated in the same host strain as the Gn/Gc-expression plasmid. To extract the plasmid, a 50-ml culture was started in LB broth supplemented with 100 µg/ml ampicillin and incubated for 18 hours at +37°C with shaking. Cells were harvested by centrifugation at 3,220 × g, +20°C, for 10 minutes, and the pellet was stored at −20°C overnight. The pellet was thawed on wet ice, and plasmids were extracted using PureLink Fast Low-Endotoxin Midi Plasmid Purification Kit (Invitrogen), following the manufacturer's protocol.

Plasmid preparations were sterilized for transfection by chloroform treatment. The mass of plasmid required for transfection was diluted into 100 µl H_2O and mixed thoroughly with an equal volume of 100% chloroform. The phases were separated by centrifugation at ~13,000 × g for 5 minutes, and the top (aqueous) phase containing the DNA was removed by pipetting and used for transfection.

Polyethyleneimine (PEI) was used to transfect mammalian cells with the Gn/Gc-expression plasmid, following the protocol described by Aricescu et al. (2006), and cultured in a medium containing 10% FBS post-transfection. Unless otherwise mentioned, 50 µg DNA and 100 µl PEI (1 mg/ml) were used to transfect a culture in a 175 cm^2 flask. When using smaller cell culture flasks, DNA and PEI amounts were scaled down proportionately to the surface area of the flask.

4.4 CONCENTRATION OF VLP SAMPLES

4.4.1 Concentration with reverse dialysis using PEG

Concentration was performed in 12–14 kDa MWCO regenerated cellulose membrane tubing (length 25 cm, diameter 29 mm), that was sealed using clamps supplied by the manufacturer of the membrane. The tubing containing the sample was laid on top of a 1-cm layer of PEG (35 kDa), and PEG was also added on top of the tubing. The sample was concentrated for 3.5 hours until the volume had reduced from 112 ml to ~6 ml, after which it was removed from tubing.

4.4.2 Concentration and buffer exchange by ultrafiltration

Amicon centrifugal filters (Merck Millipore) with the nominal molecular weight limit of 100K were used to concentrate VLP samples. Ultrafiltration apparatuses with different capacities were used depending on sample volume. Before loading the sample, filters were rinsed with buffer. The detailed centrifugation parameters for each centrifugal filter size are listed in Table S5. To remove CsCl from the CsCl density gradient fractions, up to maximum loading volume 1 × PBS was added into the filter on top of the concentrated sample, and the concentration step was repeated.

4.5 VLP SAMPLE PURIFICATION

VLPs were harvested from cell cultures by removing the culturing medium and replacing it with fresh medium. The harvested media were clarified by centrifugation at +4 °C, 3000 × g, for 30 minutes, to remove any cells or larger cell remnants. All VLP samples were stored at +4 °C following this step.

4.5.1 Dialysis

The cellulose ester dialysis tubing (diameter 20 mm) had the MWCO of either 300 kDa or 1000 kDa. It was cut to a size suitable for accommodating the sample, and pre-treated by soaking in H_2O for 15 minutes, after which the sample was loaded into the membrane tubing. Dialysis was performed at +4 °C with magnetic stirring against 200× sample volume 1 × PBS for 22.5 h. The dialyzed sample was recovered by pipetting it from the tubing.

Possible paraformaldehyde fixation during dialysis was performed by adding 0.02 % (v/v) electron-microscopy grade paraformaldehyde in the dialysis buffer. The sample was dialyzed against the paraformaldehyde solution for 22.5 h, after which excess paraformaldehyde was removed from the sample by dialysis against 1 × PBS.

Slide-A-Lyzer Dialysis Flasks, 10 K MWCO (Thermo Fischer Scientific), were soaked for 2 minutes in dialysis buffer prior to use. The sample was loaded in the flask and air was removed by submerging the flask in buffer before screwing on the cap. The samples were dialyzed against 40× sample volume 1 × PBS at +4 °C with magnetic stirring.

4.5.2 Equilibrium density ultracentrifugation with CsCl

CsCl solution used as the gradient material was prepared at the latest a day before the ultracentrifugation run by dissolving CsCl in 1 × PBS. PBS was added, until desired density (as determined by weighing 100 µl aliquots of the solution), ranging from 1.25 to 1.27 g/cm^3, was reached. The samples were ultracentrifuged using Sorvall TH660 rotor (for 4 ml tubes) or TH641 rotor (for 12 ml tubes). Either 1 or 3.7 ml of sample was added on top of either 3 ml or 8 ml of CsCl solution, respectively. The tubes were balanced by adding 1 × PBS. Ultracentrifugation was performed in a Sorvall WX Ultra 80 centrifuge at 68 706 × g, at +15 °C, for 16–17 hours. After ultracentrifugation, each sample was divided into 0.4-ml (TH660 rotor) or 1-ml

(TH641 rotor) fractions by pipetting from the surface. The fractions were weighed to determine their densities.

4.6 PROTEIN ANALYSES

4.6.1 Dot blotting

Samples were blotted manually on an Immobilon-P (0.45 µm pore size) polyvinylidene fluoride membrane. Before blotting, the membrane was activated in methanol for 15 seconds, rinsed in H_2O for 2 minutes, and in 1 × PBS for 5 minutes. The blotting stack was assembled from bottom to top starting with a few sheets of tissue paper, then two sheets of Whatman 3MM filter paper cut to the size of the membrane (the one on top was pre-wet with 1 × PBS), and finally the blotting membrane. 2–5 µl samples were pipetted on the membrane. When samples had absorbed into the membrane, it was either dried between two sheets of filter paper, or it was transferred directly to the blocking step of immunodetection.

4.6.2 Immunodetection

In case the membrane had been dried at +20 °C, it was soaked in methanol for 5 minutes prior to blocking. The wet membrane was blocked with 3% (w/v) dry skim milk in 1 × PBS, with 0.05% (v/v) polysorbate-20, at +20 °C for 1 hour. Blocking was followed by 1 hour of incubation with primary anti-Gn antibody (diluted 1:3000 in blocking buffer), 3 × 5-minute washes with 1 × PBS, 30 minutes of incubation with secondary HRP-conjugated antibody (diluted 1:5000 in blocking buffer), and 3 × 5-minute washes with 1 × PBS. The HRP conjugate was detected with ECL Western Blot substrate (Pierce), prepared according to the manufacturer's instructions. The membrane was incubated under the substrate solution for 1 minute. The blots were imaged with Bio-Rad ChemiDoc Imager, using the chemiluminescence protocol, 10–30 minutes after the application of substrate on the membrane.

4.6.3 Protein concentration measurements

Protein concentrations were measured using Bradford's method (Bradford, 1976). Samples were diluted in 20 mM Tris-HCl buffer (pH 7.5). Standard samples were prepared by diluting BSA to 1, 2, 3, and 4 µg/100 µl, and plain buffer served as a zero. 100 µl Instant Blue – Coomassie reagent (Expedeon) was added to each 100 µl sample, and absorbance values were measured with a plate reader at 595 nm. Two replicates

were made of each sample and standard. Measurements that were not in the range of the standard curve were discarded (in favor of other dilutions of the same sample).

4.7 TRANSMISSION ELECTRON MICROSCOPY

VLP samples were negatively stained for transmission electron microscopy (TEM). 3–10 µl sample was pipetted on a glow discharged, Formvar- and carbon coated 200 mesh Cu-grid and incubated for 5 minutes at ~+20 C°. Grids were washed twice in 100 µl water droplets and stained in 15 µl 2% uranyl acetate (pH 4) droplets twice, or a 30 µl droplet of 1% ammonium molybdate (pH 7), and dried using filter paper.

For immunogold labeling of the VLPs, grids were treated with antibodies before staining as follows. The grids were washed in 30 µl 1 × PBS, dried with filter paper, and blocked in a 30 µl droplet of 3% BSA for 15 minutes. Next, grids were incubated for 45 minutes in a 30 µl droplet of primary antibody solution (anti-RVFV Gn, solution diluted 1:500). After incubation, the grids were washed in 6 × 30 µl droplets of 1 × PBS. The grids were incubated in 25 µl of immunogold-labeled secondary antibody solution for 45 minutes. The grids were washed in 6 × 30 µl droplets of 1 × PBS and incubated in the last wash buffer droplet for 2 minutes before proceeding to staining.

The grids were imaged using a transmission electron microscope, either a JEOL1400 at an accelerating voltage of 80 kV, or a TECNAI F20 with an accelerating voltage of 200 kV.

4.8 IMAGE PROCESSING AND ANALYSIS

Dot blot images were analyzed by quantifying the detected signals using ImageJ. The colors of the dot blot image were inverted, background was reduced as much as possible without losing sensitivity, and the blotted areas were selected individually with a circular tool for measurement of integrated density, a unit measuring the signal intensity of the pixels in the selected area.

Transfected mammalian cell cultures were imaged 24 hours post-transfection using bright field and blue channels of a FLoid Cell Imaging Station (Thermo Fischer Scientific). Raw images from the two channels were merged to one image using ImageJ, with no further processing.

5 RESULTS

The aim of this work was to explore different production protocols to maximize RVFV VLP yield, and to optimize purification to obtain high-quality samples for electron microscopy analyses. The expression system was set up by transfecting human embryonic kidney cells with a mammalian expression plasmid based on pHL-sec, a vector optimized for expression of secreted proteins in mammalian cells (Aricescu et al., 2006). The VLP expression plasmid had been constructed by cloning an insert encoding RVFV glycoproteins Gn and Gc and the gene coding for the fluorescent marker mTurquoise into the vector (Figure 2). In this work, transfection and VLP harvest protocols were optimized, and different methods for purifying and concentrating VLP samples were examined for their efficiency (Figure 3).

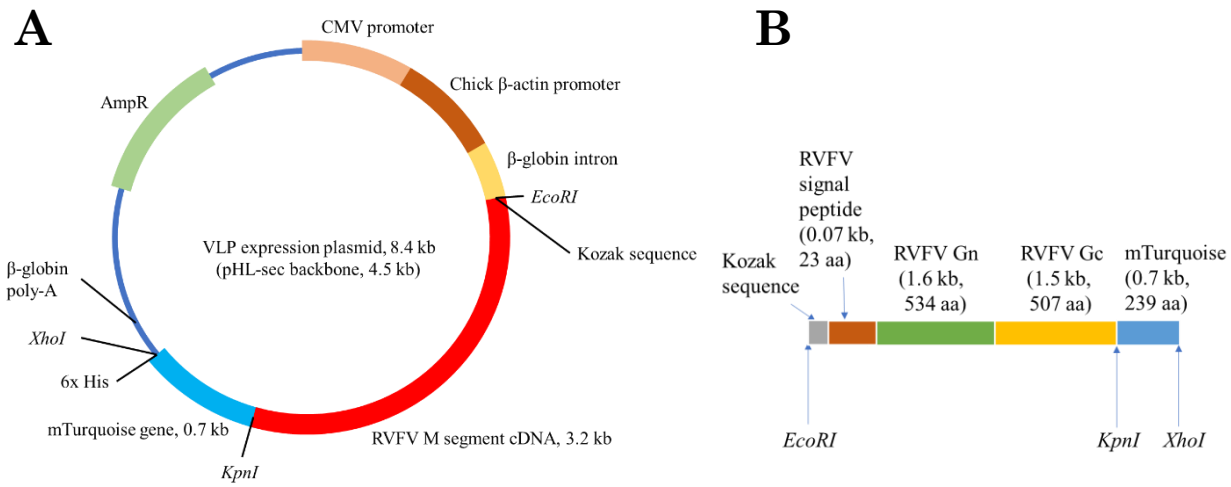

Figure 2. Features of the Gn-Gc expression plasmid. A) A map of the plasmid. *Key elements of the plasmid are indicated in the map: the insert (3.2 kb region of the RVFV M segment, encoding the RVFV glycoproteins), fluorescent tag and poly-His tag genes, selection gene, and elements enhancing mammalian expression. Important restriction enzyme recognition sites of the multiple cloning site are marked in italics. The apparent sizes of the regions are not to scale.* ***B) A linear map of the insert and mTurquoise gene.*** *The insert includes a Kozak sequence and the regions coding for a signal peptide and the glycoproteins Gn and Gc from the RVFV clone 13 M segment. Sizes of the regions and their respective products are displayed in kilobases and amino acids (apparent sizes not to scale). Key restriction enzyme recognition sites indicated in italics.*

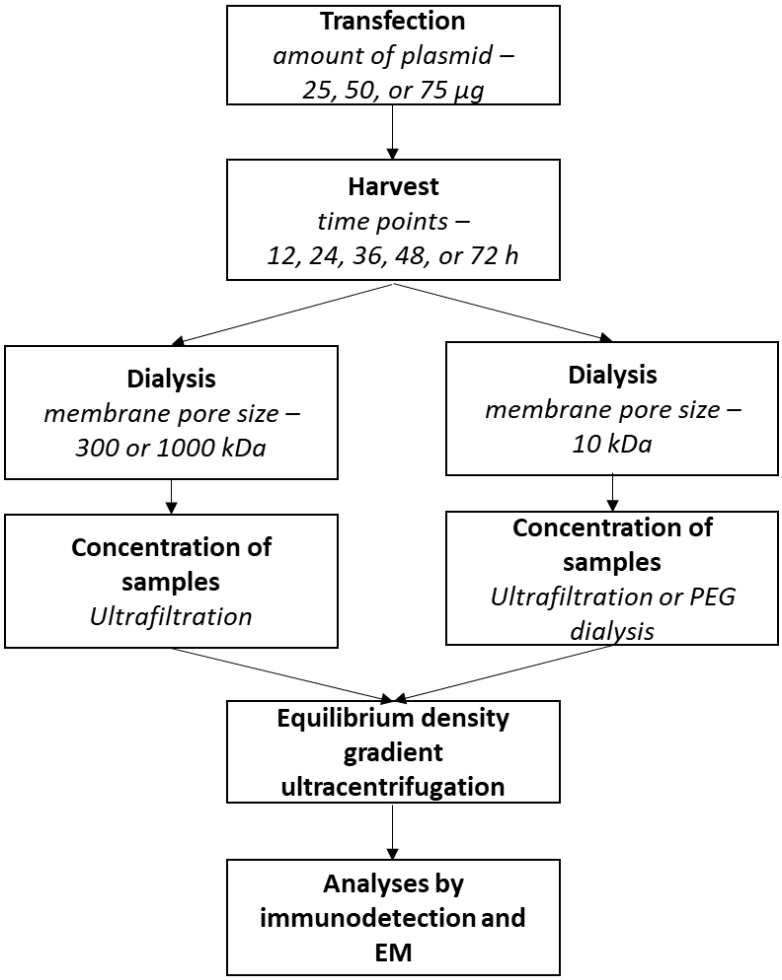

Figure 3. The workflow of VLP sample processing and targets of optimization. *Steps of the process are bolded, and the parameters that were compared and optimized are in italics.*

5.1 OPTIMIZATION OF VLP PRODUCTION

5.1.1 Plasmid gene expression detected by fluorescence microscopy

The VLP expression plasmid includes a gene coding for a fluorescent tag, mTurquoise, that is co-expressed with the VLP glycoproteins. The possibility of exploiting this tag for monitoring gene expression in cell cultures was explored by imaging transfected cultures by fluorescence microscopy. As negative controls for mTurquoise expression, cultures transfected with H_2O or a version of the VLP expression plasmid from which the mTurquoise gene had been excised were set up and imaged in parallel. The cultures were transfected following standard protocol.

The cells were imaged 24 hours post-transfection using the bright field and blue channels of the microscope. The two channels were merged using ImageJ software

(Figure 4). In the samples transfected with the VLP expression plasmid, expression of the gene of mTurquoise-tag can be observed as fluorescent dots in the cells detected by the blue channel. In contrast, no blue signals discernible from the background are found in the negative controls, confirming that cell cultures transfected with a plasmid encoding mTurquoise can be differentiated from other cultures using fluorescence microscopy (Figure 4). These results show that success of transfection and plasmid gene expression can be confirmed by microscopy before any VLP purification procedures, and without detecting VLP proteins specifically.

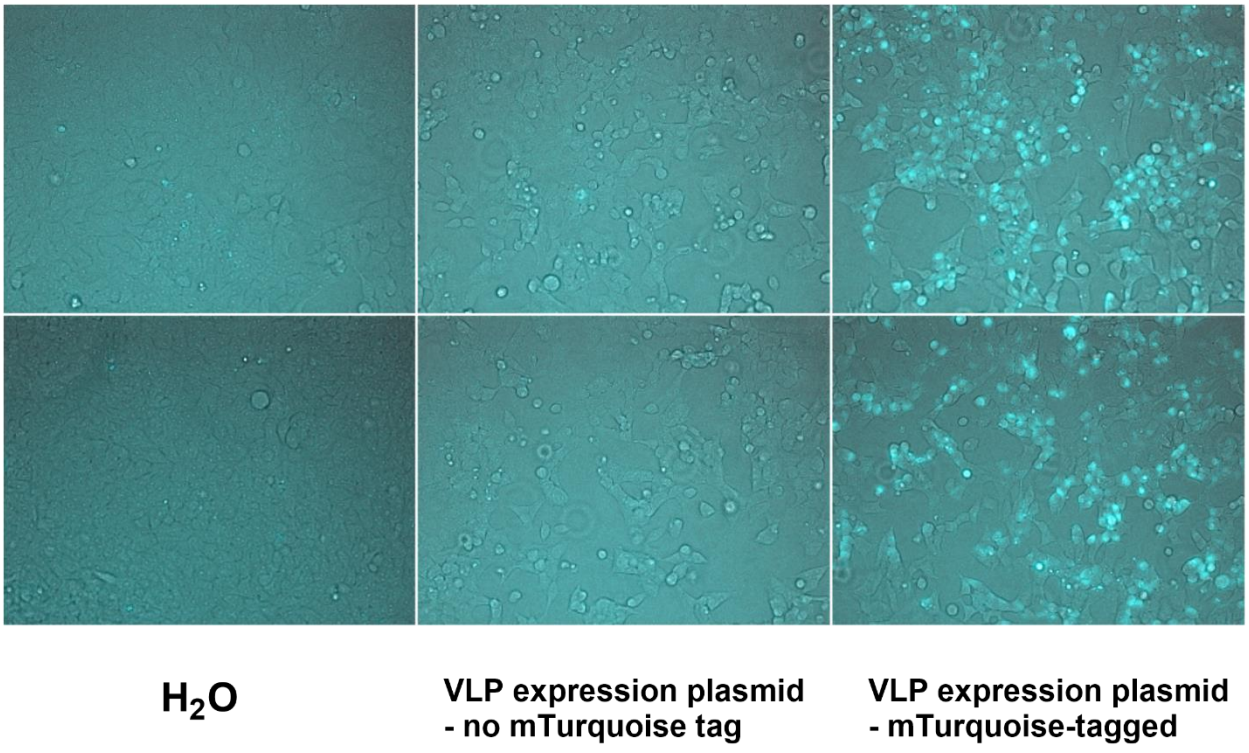

Figure 4. Success of transfection with VLP expression plasmid can be observed by fluorescence microscopy. *Columns from left to right: Controls transfected with H2O, controls transfected with tag-free VLP expression plasmid, controls transfected with VLP expression plasmid encoding the mTurquoise tag. Expression of the mTurquoise gene in the plasmid causes the distinct fluorescent signals in the blue channel of FLoid, here cyan-colored. The images are composites of blue and white channel raw images from FLoid. The two photographs per treatment are taken from two separate culture flasks.*

5.1.2 Highest RVFV Gn yield by transfecting cells with recommended plasmid amount

For optimization of the transfection procedure, different plasmid-to-cell ratios were tested. The normal 50 µg of DNA was compared with 25 µg and 75 µg of DNA per 175 cm^2 culture flask of cells, as well as a negative control with no plasmid. Four cell cultures were used for the experiment (n = 1). Seeding cell number for the cultures used in this work was an average of 3.70×10^5 cells / cm^2 of growth area (standard deviation $\pm 1.12 \times 10^5$) based on live cell count measurements performed for cultures used in three separate transfections. The cells were transfected following standard protocol. Supernatant samples were harvested at 12, 24, 36, 48, and 72 h. The samples were centrifuged, concentrated by ultrafiltration to 4% of the original volume, and analyzed by a dot blot (Figure 5). No unspecific detection by the anti-Gn antibody was observed in the blot, based on the complete absence of signal in the negative control. However, no signal can be observed in the positive controls, either, suggesting that there was a problem in the preparation of the controls.

Based on the results (Figure 5), it seems that the recommended plasmid-to-cell ratio (Aricescu et al., 2006) is also optimal for the expression of the VLPs. With higher DNA-to-cell ratios (75 µg), the expression begins as more or less equally strong than that of the samples transfected with the recommended ratio. At 72 hours, however, the Gn expression seems to drop in the samples transfected with 75 µg of DNA. Using only half of the recommended amount of plasmid DNA in transfection (25 µg) seems only to decrease expression, as expected. The recommended ratio of 50 µg plasmid DNA per 175 cm^2 cell culture flask was used in all subsequent transfections.

5.1.3 RVFV Gn expression highest at 36-72h

In order to study the production of VLPs at different time points in adherent mammalian cell cultures, Gn expression levels were analyzed in time points 12 h, 24 h, 36 h, 48 h, and 72 h. VLPs were produced in mammalian cells by transfecting the cells with the VLP expression plasmid, or H_2O (negative control for expression). Supernatant samples were harvested at the indicated times, centrifuged to remove cells, concentrated by ultrafiltration to approximately 4% of original volume, and analyzed with a dot blot assay (Figure 5A). The signals in the dot blot image were

quantified densitometrically using ImageJ software (Figure 5B). The signal intensity analysis helps gauge the best harvest times for optimal yield of RVFV VLPs. Some level of Gn expression is observed already at 24 hours (Figure 5), but the most favorable harvest times seem to be at 36, 48 and 72 hours, when the expression of RVFV Gn is at its peak. There is no notable difference between 36, 48, and 72 hours.

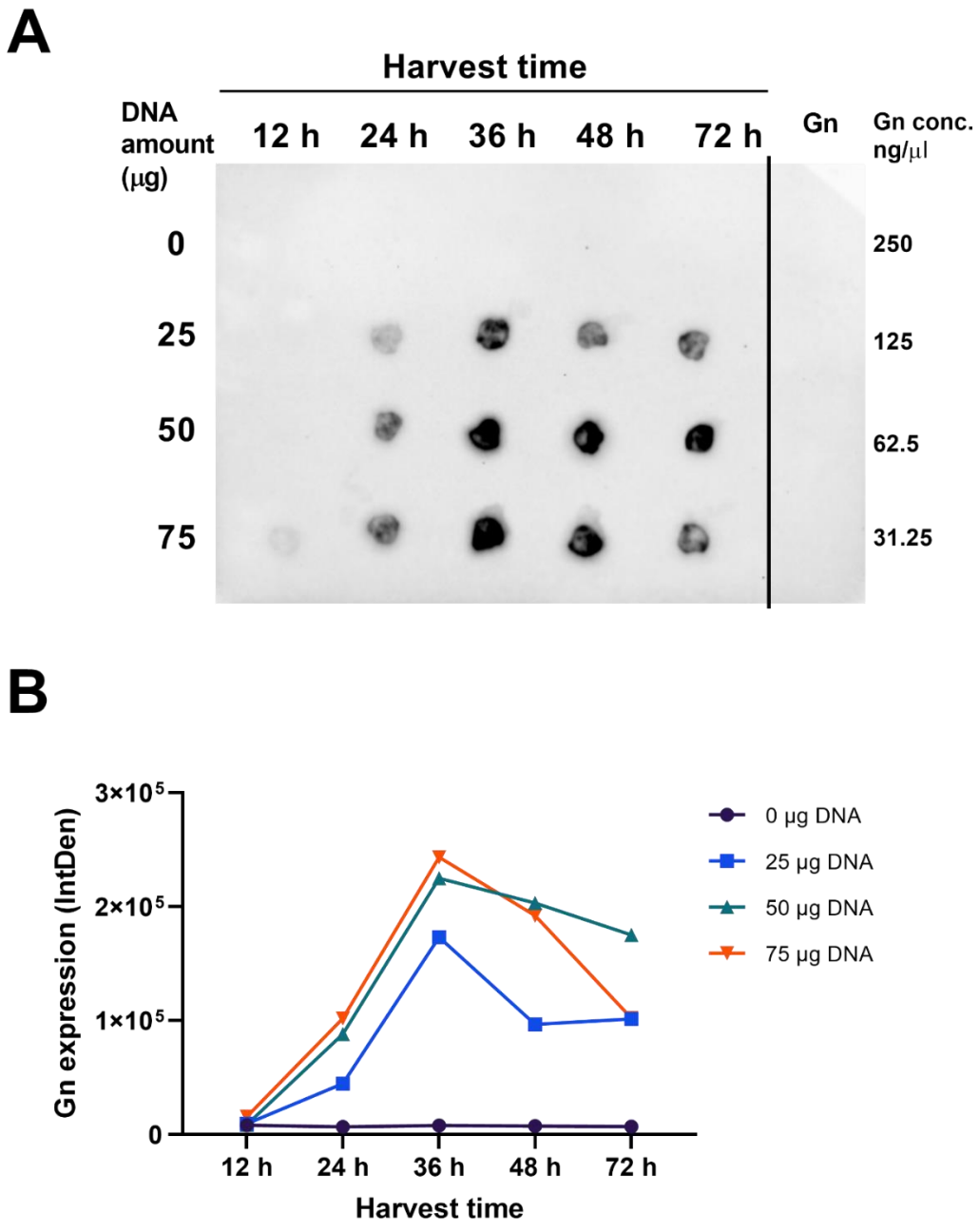

Figure 5. Effect of harvest times and plasmid DNA amounts on Gn expression. A) Dot blot analysis. *Samples harvested at 5 time points and from 4 differently treated cell cultures (with varying amounts of plasmid used in transfection). 5 µl of each concentrated sample was blotted, n = 1. The positive controls (Gn dilution series) were not visible in the blot image.* ***B) Measurements from a densitometric analysis of the dot blot image (A).*** *The graph displays the relationship between Gn signal intensity and harvest time in the 4 cell cultures. On the vertical axis, IntDen (integrated density) represents color and abundance of pixels in a certain area as measured by the image analysis software.*

5.2 VLP PURIFICATION CHALLENGING BY EQUILIBRIUM GRADIENT ULTRACENTRIFUGATION

Equilibrium density gradient ultracentrifugation can be used to separate biological materials based on differences in density (Frei, n.d.). To examine the possibility of purifying and concentrating VLPs by applying a CsCl equilibrium density gradient, and to control for factors that might affect the performance of this method, four different samples were prepared for ultracentrifugation. The pore size of the dialysis membrane determines how much material is removed from the sample during dialysis, and the role of fixatives is to stabilize the structure of VLPs. The effect of the use of a chemical fixative as well as the pore sizes of the dialysis membranes on the movement of the particles in CsCl gradient were assessed.

75 ml VLP culture supernatant and 25 ml negative control culture supernatant were harvested 48 h post-transfection. The samples, excluding negative control, were pooled to eliminate the possible differences in expression between individual cell culture flasks. The VLP culture supernatant sample was divided into 25 ml aliquots that were subjected to three different treatments. One of the aliquots was dialyzed using a membrane with a molecular weight cutoff value (MWCO) of 1,000 kDa (sample 1000). The other two aliquots were dialyzed using a membrane with a MWCO of 300 kDa. One of these was dialyzed without a fixative (sample 300), while the other was treated with a fixative by adding 0.02% paraformaldehyde in the dialysis buffer (sample 300-PFA). The negative control (sample C) was dialyzed with a 300 kDa membrane.

After dialysis, the samples were concentrated by ultrafiltration, separated in an equilibrium density gradient using CsCl solution with an average density of 1.25 g/cm^3, and fractionated. Before fractionation, centrifugation tubes were examined under white light to find any light scattering zones that could correspond to VLPs, but no zones absent from the negative control were observed in the samples. A graph plotted from the densities of each fraction (Figure 6A) shows that the linear density gradient formed successfully during the ultracentrifugation, with only slight irregularities.

To analyze the fractions using immunodetection, they were concentrated by ultrafiltration. A de-salting step was applied in the concentration process to remove

most of the CsCl from the fractions. The fractions were analyzed in a dot blot assay to examine the abundance of RVFV Gn in each fraction (Figure 6B). Strong Gn signals were detected in many fractions in all transfected samples, especially in low density fractions (1-6), with the signals gradually weakening towards the bottom of the tube. Differences between sample treatments were not pronounced. It might be worth noting that in sample 1000, Gn signal was observed in only 9 fractions instead of 10 (as was the case of samples 300 and 300-PFA). PFA-treatment did not seem to affect the density of the particle and thus the migration of the particles in the gradient. Based on these results, it is difficult to exactly determine the fraction where the VLPs can be found, as the signal seems equally strong across several fractions (Figure 6B; sample 300, 2-4). The three strongest signals correspond to density values in the range of 1.06–1.13 g/cm^3 (Figure 6).

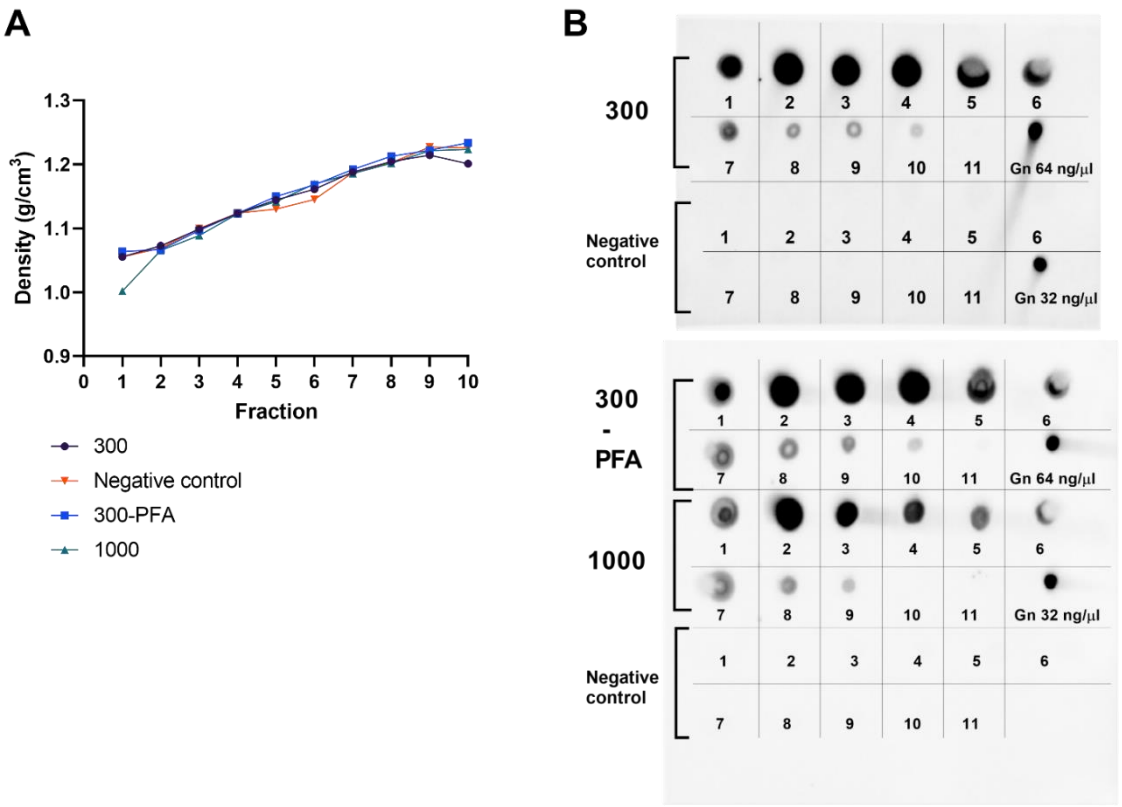

Figure 6. Analysis of fractions from CsCl density gradient ultracentrifugation. *Four samples were ultracentrifuged and fractionated: a VLP expression sample dialyzed with a 300 kDa MWCO membrane (300), a VLP expression sample dialyzed with a 300 kDa MWCO membrane and fixed with PFA (300-PFA), a VLP expression sample dialyzed with a 1,000 kDa membrane (1000), and a negative control sample, with no DNA used in transfection, dialyzed with a 300 kDa MWCO membrane.* ***A) Density gradient plotted from density measurements of fractions.*** *The density of each fraction from 1 to 10 is plotted in the y-axis. The gradients display some irregularities but are roughly linear.* ***B) Dot blot analysis of fractions.*** *Gn protein samples diluted to 64 and 32 ng/µl served as positive controls for immunodetection. Gn signal is strong across several fractions in all fractionated samples.*

5.3 ULTRAFILTRATION LEADS TO BETTER FRACTIONATION OF RVFV GN THAN DIALYSIS AGAINST PEG

The volumes of the dialyzed samples of cell culture medium needed to be reduced for ultracentrifugation. Additionally, analyses based on immunodetection required samples with higher concentrations of RVFV Gn than that of the dialyzed, unconcentrated medium, so that the Gn protein on the VLP surface could be detected. Two methods for reducing sample volume were compared by immunodetection of RVFV Gn present in the samples after the respective concentrating processes and ultracentrifugation. The methods tested here were ultrafiltration by centrifugal filters and reverse dialysis against polyethylene glycol (PEG) through a semipermeable membrane.

To examine the possibility of either treatment affecting the separation of the sample in a density gradient, samples concentrated by the two methods were purified by equilibrium gradient ultracentrifugation. The VLP samples were produced in cell cultures, following standard protocols. Culture supernatants harvested at 24, 48, and 72 h post-transfection were pooled together, resulting in 225 ml supernatant. The supernatant sample was dialyzed in a regenerated cellulose membrane flask with 10 kDa MWCO against 1 × PBS. The dialyzed sample was divided in two 112 ml aliquots. One of these was concentrated to 6 ml by ultrafiltration using an Amicon Ultra-15 100 K unit. The other aliquot was concentrated by PEG dialysis. The sample was transferred to a 12–14 kDa regenerated cellulose membrane and the sample was concentrated to 6 ml.

A negative control had been prepared in parallel with the VLP expression cultures by starting a new culture in a 75 cm^2 flask and transfecting it with 7.5 µg of control plasmid (pKSII) that does not encode any RVFV proteins. Harvests were performed as described for the VLP samples, resulting in 30 ml of sample, which was not dialyzed, but concentrated with an Amicon Ultra-15 100K device to 1.5 ml.

The samples were subjected to CsCl density gradient ultracentrifugation, using CsCl solution with the average density of 1.27 g/cm^3. Each sample was divided in two equal aliquots whereas the negative control with a smaller volume of starting material in

only one. Following ultracentrifugation, the samples were divided into 1 ml fractions (Figure S1) and concentrated by ultrafiltration.

The fractions concentrated by ultrafiltration were analyzed by immunodetection in a dot blot (Figure 7). There was an unusually high background signal in the blot, but general interpretation of the results was still possible. Both samples showed poor fractionation with regard to Gn, with the slight difference that the Gn in the PEG-dialyzed sample was found even in the densest fractions (10–12). In the sample initially concentrated with ultracentrifugation, Gn was not detected in these three bottom fractions, excluding a weak signal in the bottom fraction. There is a possibility that PEG treatment interferes with VLP movement in equilibrium density gradient.

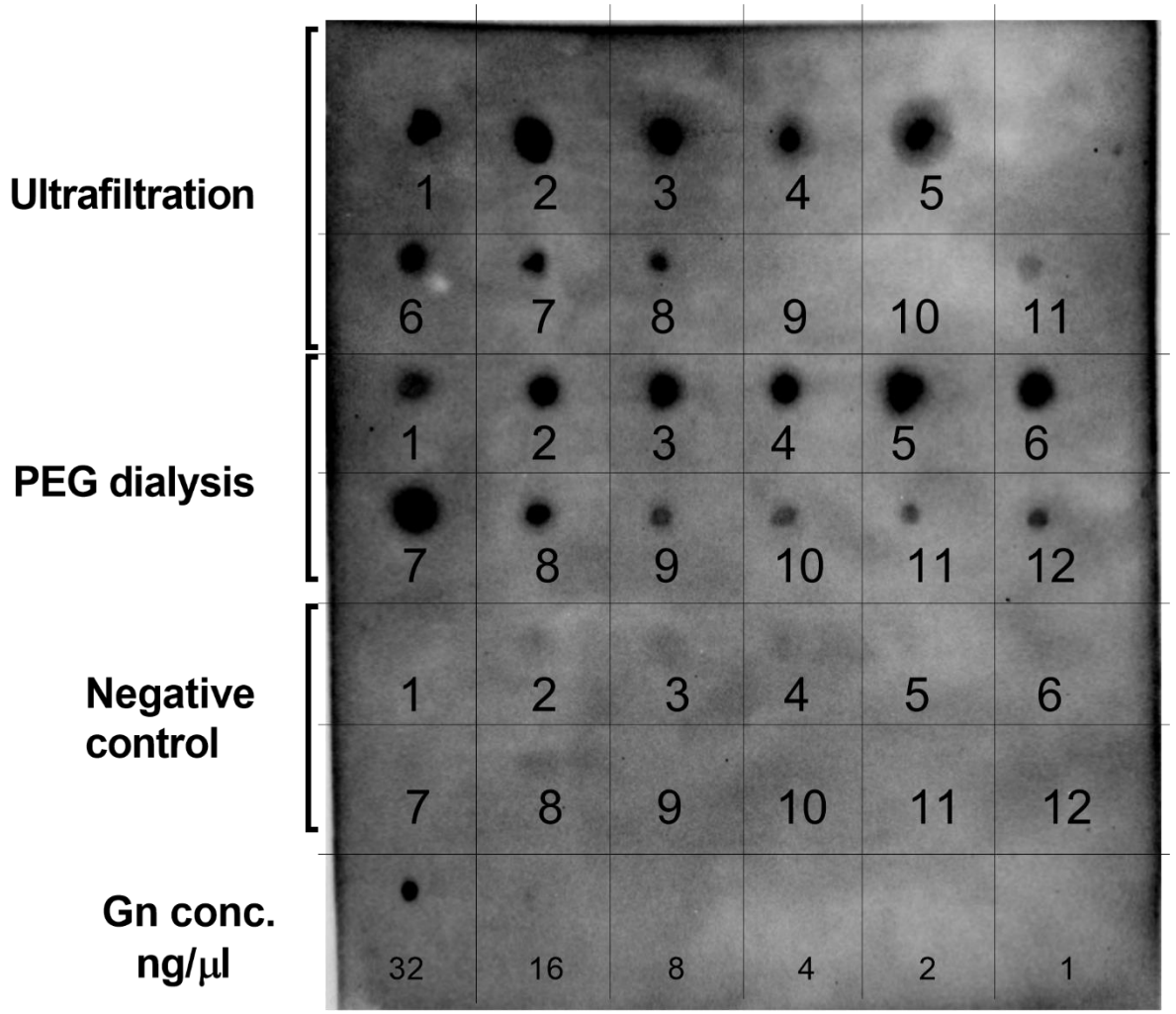

Figure 7. Effect of concentration methods in Gn content of CsCl gradient fractions. *Dot blot analysis of fractions. 2µl of each fraction was blotted. Three samples had been fractionated: a sample concentrated by PEG dialysis (PEG), a sample concentrated by ultrafiltration (Ultrafiltration) and a negative control sample, with no DNA added in transfection, concentrated by ultrafiltration (Negative control). A Gn dilution series served as the positive control. (Only 32 ng/µl dilution visible). In the sample concentrated by ultrafiltration, Gn was not found in fractions 9 and 10, whereas in the PEG dialyzed sample Gn was found in all fractions.*

5.4 VLPS DETECTED BY IMMUNO-EM IN PURIFIED AND CONCENTRATED SAMPLES

Selected fractions obtained from equilibrium gradient separation in this work were analyzed with electron microscopy (EM) to examine their VLP content. Fractions with a high Gn content (based on immunodetection results; see Figures 6 and 7) were chosen for grid preparation and EM. The protein concentrations of the fractions were determined by Bradford's method. During microscopy, particles with a diameter of roughly 100 nm were searched, as the size of RVFV particles has been reported to be 80–120 nm (Halldorsson et al., 2018).

Fractions 2-5 (Figure 6) from the CsCl gradients of samples 300, 300-PFA, and 1000, were selected, diluted to 1 mg/ml and stained with uranyl acetate for EM analysis. In the micrographs, various types of materials can be seen, possibly including cell membrane remnants, extracellular vesicles (EVs), or VLPs (Figure 8). Other vesicle structures, such as EVs secreted by the host cells, might be falling in the same range of size and shape as the VLPs (van Niel et al., 2018). Thus, differentiating between VLPs and EVs reliably was not possible by this method. In fraction n:o 5 of the PFA-treated sample dialyzed with a 300 kDa membrane, one very spherical vesicle with a regular surface structure could be observed (Figure 8A). Based on its size (~100 nm), it could be a VLP, but without means to analyze the surface structure of the vesicle more closely, its identity could not be conclusively determined.

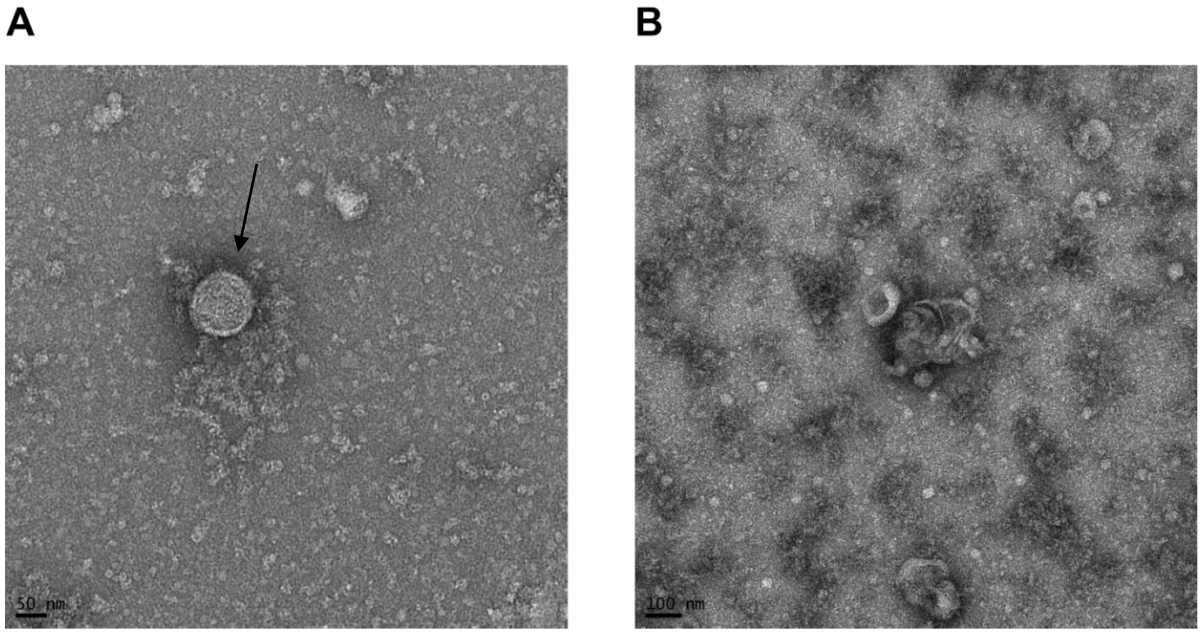

Figure 8. TEM micrographs of samples stained with 2% uranyl acetate. *A) A possible VLP in PFA-fixed CsCl fraction 5 from a 300 kDa-dialyzed sample (indicated with an arrow). Size of the particle corresponds to RVFV particle size of approximately 100 nm. B) 1000 kDa -dialyzed sample, CsCl fraction 3. In this micrograph, diverse structures can be observed that may be large proteins, cell membrane fragments, VLPs, or extracellular vesicles.*

Two independent sets of VLP samples were analyzed by immunoelectron microscopy (immuno-EM), which is a way of identifying the RVFV VLPs specifically in the samples. The VLP sample grids can be treated with the RVFV Gn antibody, and a secondary antibody conjugated with electron-opaque gold nanoparticles to enable detection of antibody binding by EM (Murtey, 2016). Differentiation between VLPs and extracellular vesicles is possible by observation of the vesicles associated with gold particles. For the purposes of this analysis, any vesicle-like structure with several gold particles visibly attached was considered a VLP.

The first set of immuno-EM samples was selected from the fractions that had already been analyzed by negative staining TEM. These had been dialyzed with cellulose ester membranes (pore size either 300 kDa or 1000 kDa), concentrated by ultrafiltration, run into a CsCl gradient, and fractionated. Fractions 2-5 from all samples, except the negative control, were analyzed (immunodetection analysis of fractions, see Figure 6). Microscopy of the first set of samples revealed very few VLPs, one of which is shown in Figure 9D. Otherwise, the gold particles found in the samples were associated with diverse non-spherical membrane structures, or with no visible structure at all.

Several VLPs were observed by EM in the second set of samples (Figure 9, A-C) originating from a separate batch of transfection. The samples were dialyzed with a dialysis flask (regenerated cellulose membrane, MWCO of 10 kDa), concentrated by either ultrafiltration or PEG reverse dialysis, fractionated following a CsCl density gradient ultracentrifugation (Figure 7), and concentrated by ultrafiltration before microscopy. The fractions were diluted 1:4 in 1 × PBS to reduce sample viscosity, and 10 µl sample was then loaded on the grid. VLPs found in this round of microscopy were irregularly shaped and most often appeared as aggregates of three to five particles (Figure 9, A-C). VLPs were found more often, compared to the previous set of samples, but they were still not sufficiently abundant on the grids for efficient cryo-EM data collection. Preliminary observations made by cryo-EM of these samples (data not shown) revealed a high density of proteins, whereas VLP-like structures were scarce.

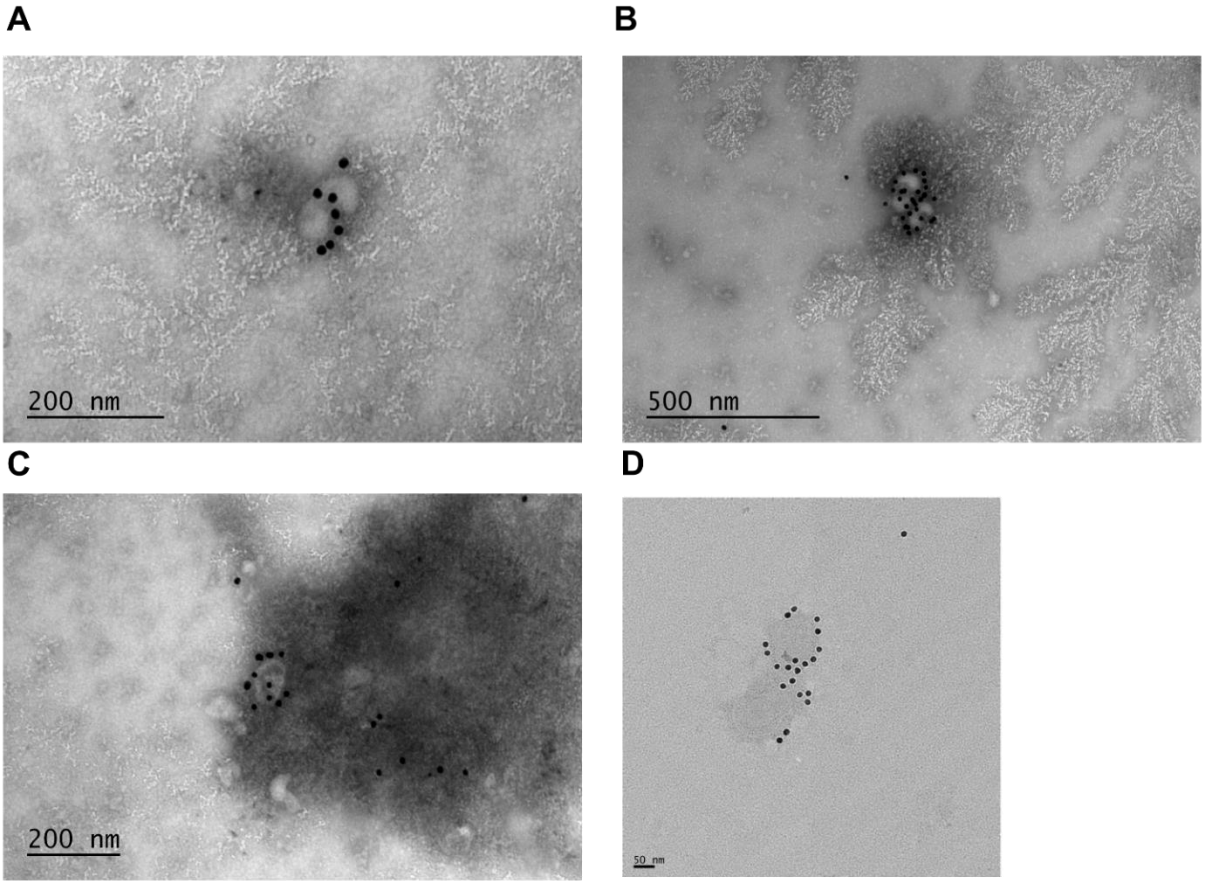

Figure 9. TEM micrographs of immunogold-labeled samples stained with 1% ammonium molybdate. *The electron-opaque gold particles mark the outlines of VLPs. The sizes of the particles correspond to RVFV size (around 100 nm). A) – C) Sample dialyzed with a regenerated cellulose membrane, 10 kDa, concentrated by ultrafiltration, CsCl fraction 5. D) TEM micrograph of immunolabeled VLPs from 300 kDa dialyzed, unfixed sample, CsCl fraction 2.*

6 DISCUSSION

VLPs are a promising alternative for studying surface structures of pathogenic viruses such as RVFV, the handling of which would otherwise be very laborious. VLPs are non-infectious and potentially easy to both produce and purify. Their envelope is expected to look very similar, if not identical, to that of an infectious virus, including RVFV virion. In earlier studies, contradicting results have been obtained on whether expression of RVFV Gn and Gc, without other viral components, can lead to production of RVFV VLPs (Habjan et al., 2009; Mandell et al., 2010a). The possibility of the purification of RVFV VLPs suitable for cryo-EM analyses had not been examined in these studies. For this purpose, the initial yields of VLPs should be high, and the elimination of EVs and other membranous material abundant in the samples might be difficult without damaging the VLPs.

This work describes the attempts to optimize protocols for purification of RVFV VLPs produced in mammalian cell cultures for structural analyses. In this work, RVFV VLPs were identified by immunoelectron microscopy, confirming that the VLPs can be processed for electron microscopy analyses using the methods described here. There are still open questions remaining, most importantly those of VLP yield and sample purity, which should be answered before the methods can be applied in a larger scale for structural studies.

Developing the methods for the production and purification of RVFV VLPs involves some challenges. One of them is the very nature of VLPs: their lack of genome prevents their detection and quantification with methods traditionally applied for viruses, such as infectivity assays and nucleic acid analyses (Steppert et al., 2017). In this work, the expression of viral genes cloned in a mammalian expression vector for VLP production was initially confirmed by fluorescence microscopy. The quality of the images was low, which might be attributed to the fact that the parameters of the blue channel (excitation 390/40 nm, emission 446/33 nm) used for capturing mTurquoise fluorescence overlaps poorly with the respective spectra of mTurquoise (excitation 434 nm, emission 474 nm) (Goedhart et al., 2010). Images more suitable for quantitative applications may be obtained by using a fluorescence microscope that has a filter set for mTurquoise.

Antibody-based detection was used to evaluate the presence and relative abundance of VLPs. The anti-RVFV-Gn antibody that was used here (Allen et al., 2018) exclusively recognizes the native conformation of RVFV Gn. This precludes applying immunodetection methods that denature the target proteins, such as Western blot (Ilona Rissanen, personal communication). Therefore, dot blots were used in this work for Gn detection. However, interpretation of the results obtained by immunodetection should be cautious, because in addition to VLPs, the Gn protein antigen used for the detection during the purification optimization is most likely present in nonspecific membrane structures as well. The presence of VLPs was confirmed using immuno-EM, which allows Gn proteins of VLPs to be distinguished from Gn bound to other membrane structures. In the future, more precise and less invasive methods, such as nanoparticle tracking or multi-angle light-scattering detection, could be applied for VLP quantification (Steppert et al., 2017). Nevertheless, Gn is a strong indicator for the presence of VLPs, and the expression of RVFV glycoproteins is a prerequisite for VLP formation.

In earlier research by Mandell et al. (2010a), RVFV Gn expression in a comparable HEK293 platform was determined to be highest 36–60 hours post-transfection. Using a modified cell line in the adherent cultures (HEK293-gag cells that express Moloney murine leukemia virus gag protein) did not considerably enhance VLP production (Mandell et al., 2010a), and for this reason, gag-producing cell lines were not tested in this work. HEK293T cells were used in the experiments described here, as recommended for the pLEXm-derived vector used (Aricescu et al., 2006). For our expression system, the best times for harvesting the VLP samples were estimated to be 36–72 hours post-transfection, based on the results of the preliminary VLP production experiment. This is in accordance with the results obtained by Mandell et al (2010a). The DNA-to-cell ratio recommended by the original publication describing the transfection protocol used in this study (Aricescu et al., 2006) seemed optimal for strong and sustained Gn expression.

When evaluating the results from the time course and transfection experiments, it should be considered that Gn controls were not visible on the blot, possibly owing to a mistake in the preparation of controls. Therefore, it remains open whether there is a linear relationship between Gn concentration and signal intensity in the dot blot. This

should be determined in future experiments by including a standard curve based on serial dilutions of Gn. Moreover, statistical analysis to assess whether the differences between treatments are significant could not be performed based on these results. This is due to the time frame of the thesis that did not allow repeating the experiment or producing replicate samples. However, these preliminary results will help guide the design of further experiments. To further test the effects tentatively observed here, simultaneous culturing of several separate cell cultures for each treatment would enable statistical analyses of the results. Cell density of the cultures should also be standardized to ensure comparable protein production between cultures. Additionally, the VLP preparations obtained from the time course experiment could be analyzed by immuno-EM to examine the abundance of intact VLPs that egress from the cells during each time window.

Effective purification and concentration of samples is essential to obtain high-quality samples for structural studies by cryo-EM (Stark & Chari, 2016). Some degree of VLP loss during purification is inevitable, regardless of the purification methods used, but certain methods might perform more efficiently than others. After removing cells from samples of culturing medium by low-speed centrifugation, large cell remnants, such as membrane fragments and extracellular vesicles, can still be found in abundance. The elimination of these materials by methods such as dialysis against PBS and equilibrium density gradient ultracentrifugation considerably facilitates examining the VLPs by EM. The permeability (pore size) of dialysis membranes composed of the same material did not seem to have a notable effect on purification, whereas it seemed that membrane material of the dialysis tubing might affect VLP yield, based on preliminary observations in immuno-EM. Fewer VLPs were detected by EM in samples dialyzed using cellulose ester membranes, compared with regenerated cellulose membranes, although this contrast might depend entirely on the different volumes of starting material. However, to avoid loss of VLPs during dialysis, the effect of dialysis membrane composition should be investigated systematically by dialyzing similar volumes of starting material with dialysis membranes of different material but equal permeability.

The reduction of dialyzed supernatant volume prior to ultracentrifugation was approached with two alternative methods, of which PEG dialysis seemed to perform

more weakly compared to ultrafiltration. After ultracentrifugation, Gn signal in the PEG-dialyzed sample was divided across all fractions, while signal was not found in the bottom three fractions of the ultrafiltrated sample. This suggests that PEG might interfere with sample fractionation in some manner. One caveat of this experiment was that the two concentration methods were not analyzed directly after the concentration processes, preventing feasible quantitative comparisons of total Gn content between samples. This should be addressed by analyzing the samples before any downstream processing by dialysis of ultracentrifugation. Further analyses, including comparison with other concentration methods, such as vacuum concentration, could be useful in determining the best method of reducing sample volume.

The results obtained here indicate that VLPs do not separate readily in a CsCl density gradient, rendering the benefits of this purification step uncertain. RVFV buoyant density has been reported as 1.16–1.18 g/ml (Ikegami et al., 2005), or 1.20–1.21 g/ml by Springer Index of Viruses (Michèle Bouloy, 2011). Buoyant densities of extracellular vehicles (EVs) range from 1.08 g/ml to 1.22 g/ml (Renner et al., 2018). Therefore, many EVs could co-localize with VLPs in CsCl gradient. There is a possibility that the samples analyzed here were too concentrated and crowded with cell debris, EVs, and VLPs, which could have prevented efficient separation of sample contents. It is also likely that the presence of Gn signal in immunodetection does not directly correlate with VLPs, as the signal might also originate from Gn associated with other membrane structures.

Instead of equilibrium density gradient ultracentrifugation, VLPs could be extracted from samples by pelleting them through a sucrose cushion, as has been done with RVFV virions (Halldorsson et al., 2018) and RVFV VLPs (Mandell et al., 2010a) before, but this would risk damaging the possibly fragile structure of the VLPs. Unless fine-tuning of the purification protocols described in this thesis improves the quality of VLP samples, alternative purification methods, that are not based on ultracentrifugation, should be considered. Recently, a combination of size-exclusion and heparin affinity chromatography was successfully applied for separating HIV-gag VLPs from EVs (Reiter et al., 2019), and this promising method should be tested for extraction of RVFV VLPs.

VLP appearance and abundance in samples were examined by immunoelectron microscopy, a straightforward and relatively rapid procedure. So far, VLPs have been scarce on the grids, often aggregated, and irregularly shaped, all of which makes collection of structural data more challenging. Upscaling of VLP expression cultures and experimenting with different purification protocols might help to increase VLP frequency on the grids. To preserve a symmetrical surface structure for cryo-EM, the VLPs could be treated with a fixative agent such as PFA (Halldorsson et al., 2018). Unfortunately, no VLPs were observed in the immuno-EM analysis of the PFA-treated samples produced in this work, so new PFA-treated VLP samples should be prepared and analyzed to test this hypothesis.

There are alternative approaches to the preparation of cryo-EM grids that might prove valuable for developing RVFV VLP sample preparation. Some biomaterials, possibly including the VLPs processed in this work, can be corrupted by conventional purification methods. Lengthy purification steps may also introduce artifacts and favor non-native conformations (Stass et al., 2018). It would therefore be advantageous if the VLPs could be attached to the cryo-EM grid directly from the biological source, such as cell culture medium, without extra purification steps. Antibody-affinity grids have been applied for this purpose: monoclonal antibodies targeting the sample are attached to the grid, and the antibody-antigen interaction effectively locks the target biocomplex in place for imaging (Yu et al., 2016).

Sample capture methods relying on antibody-affinity could be further refined by taking advantage of covalent interactions. Spy-tag Spy-Catcher technology (Reddington & Howarth, 2015) can be used for covalent and irreversible conjugation of proteins. By coating the grid with SpyCatcher proteins, the target material could be captured by recombinant antibodies equipped with SpyTag. To streamline the process, antibodies could even be eliminated from the equation by incorporating the SpyTag directly into the target molecules, such as the envelope proteins of RVFV VLPs. There is, however, a possibility that the incorporated tag would interfere with the ultrastructure of the VLP surface.

RVFV VLPs have several potential applications in structural research. VLPs can be used for studying the glycoprotein shell of RVFV and its interactions with host

systems, such as host receptor binding and viral fusion with endosomes. Fusion intermediates of RVFV can be studied by modelling endosomes with synthetic liposomes, extending the work of Halldorsson et al. (2018). In-cell cryotomography, accompanied by focused ion-beam milling to produce electron-permeable sections of cells, would be the more ambitious and labor-intensive approach to follow the fusion process or VLP formation in its natural context within cells (Pfeffer & Mahamid, 2018). The exact mechanisms of prospective antivirals could also be examined: several antiviral small molecules and peptides show promise for preventing infection by blocking RVFV fusion (Atkins & Freiberg, 2017), and understanding their function could aid in the intelligent design of new antivirals.

One important application for the structural characterization of a pathogenic virus is examining the neutralizing mechanisms of antibodies raised to combat infection. The structures and binding sites of certain antibodies specific to the soluble or adenovirus-conjugated forms of RVFV Gn and Gc have been analyzed by Hao et al., (2020), Wang et al. (2019), and Allen et al. (2018). Wang et al. (2019) noted that they recovered only one antibody raised against Gc, which might be due to some Gc-specific antibodies targeting conformations other than that of the isolated protein (Wang et al., 2019). This highlights the potential of VLPs for representing the native conformation of the viral glycoprotein shell when structurally characterizing antibody-antigen complexes. New neutralizing antibodies targeting the native conformation of viral glycoproteins could also be produced by using VLPs to mimic the native antigenic surface of RVFV. RVFV VLPs have been shown to elicit humoral immune responses in animal models (Mandell et al., 2010a; Näslund et al., 2009), and antibodies could be isolated from animals immunized in this way, without causing RVFV infection.

Taken together, the results presented here give valuable insight on RVFV virus-like particle sample processing for structural analyses. A streamlined protocol for processing the VLPs from a plasmid construct to cryo-EM micrographs will greatly facilitate research on the structural properties of the RVFV glycoprotein shell. With further optimization of the procedures described here, or the application of alternative methods, the production of RVFV VLPs has great potential to accelerate structural studies of RVFV and development of much-needed therapeutics and vaccines. Applied

to other enveloped RNA viruses, similar approaches might have a significant impact on the field of structural virology.

7 ACKNOWLEDGEMENTS

I would like to extend my sincere appreciation towards my supervisors, Juha Huiskonen and Elina Roine, for their support and guidance. I also want to thank my coworkers at the lab for their help and good advice, and my friends and family for their encouragement.

8 REFERENCES

Abudurexiti, A., Adkins, S., Alioto, D., Alkhovsky, S. V., Avšič-Županc, T., Ballinger, M. J., Bente, D. A., Beer, M., Bergeron, É., Blair, C. D., Briese, T., Buchmeier, M. J., Burt, F. J., Calisher, C. H., Cháng, C., Charrel, R. N., Choi, I. R., Clegg, J. C. S., de la Torre, J. C., … Kuhn, J. H. (2019). Taxonomy of the order Bunyavirales: update 2019. *Archives of Virology*, *164*(7), 1949–1965. https://doi.org/10.1007/s00705-019-04253-6

Allen, E. R., Krumm, S. A., Raghwani, J., Halldorsson, S., Elliott, A., Graham, V. A., Koudriakova, E., Harlos, K., Wright, D., Warimwe, G. M., Brennan, B., Huiskonen, J. T., Dowall, S. D., Elliott, R. M., Pybus, O. G., Burton, D. R., Hewson, R., Doores, K. J., & Bowden, T. A. (2018). A Protective Monoclonal Antibody Targets a Site of Vulnerability on the Surface of Rift Valley Fever Virus. *Cell Reports*, *25*(13), 3750–3758. https://doi.org/10.1016/J.CELREP.2018.12.001

Aricescu, A. R., Lu, W., Jones, E. Y., & IUCr. (2006). A time- and cost-efficient system for high-level protein production in mammalian cells. *Acta Crystallographica Section D Biological Crystallography*, *62*(10), 1243–1250. https://doi.org/10.1107/S0907444906029799

Atkins, C., & Freiberg, A. N. (2017). Recent advances in the development of antiviral therapeutics for Rift Valley fever virus infection. *Future Virology*, *12*(11), 651–665. https://doi.org/10.2217/fvl-2017-0060

Bouloy, Michèle. (2011). Phlebovirus. In C. Tidona & G. Darai (Eds.), *The Springer Index of Viruses* (pp. 223–229). Springer New York. https://doi.org/10.1007/978-0-387-95919-1_32

Bouloy, Michele, & Weber, F. (2010). Molecular biology of rift valley Fever virus. *The Open*

Virology Journal, *4*, 8–14. https://doi.org/10.2174/1874357901004020008

Bradford, M. (1976). A Rapid and Sensitive Method for the Quantitation of Microgram Quantities of Protein Utilizing the Principle of Protein-Dye Binding. *Analytical Biochemistry*, *72*(1–2), 248–254. https://doi.org/10.1006/abio.1976.9999

Faburay, B., Labeaud, A. D., Mcvey, D. S., Wilson, W. C., & Richt, J. A. (2017). Current Status of Rift Valley Fever Vaccine Development. *Vaccines*, *5*(3), 29. https://doi.org/10.3390/vaccines5030029

Frei, M. (n.d.). *Centrifugation Separations including CsCl gradient centrifugation*. BioFiles, Sigma-Aldrich. Retrieved April 22, 2020, from https://www.sigmaaldrich.com/technical-documents/articles/biofiles/centrifugation-separations.html

Goedhart, J., van Weeren, L., Hink, M. A., Vischer, N. O. E., Jalink, K., & Gadella, T. W. J. (2010). Bright cyan fluorescent protein variants identified by fluorescence lifetime screening. *Nature Methods*, *7*(2), 137–139. https://doi.org/10.1038/nmeth.1415

Habjan, M., Penski, N., Wagner, V., Spiegel, M., Överby, A. K., Kochs, G., Huiskonen, J. T., & Weber, F. (2009). Efficient production of Rift Valley fever virus-like particles: The antiviral protein MxA can inhibit primary transcription of bunyaviruses. *Virology*, *385*(2), 400–408. https://doi.org/10.1016/j.virol.2008.12.011

Halldorsson, S., Li, S., Li, M., Harlos, K., Bowden, T. A., & Huiskonen, J. T. (2018). Shielding and activation of a viral membrane fusion protein. *Nature Communications*, *9*(1), 349. https://doi.org/10.1038/s41467-017-02789-2

Hao, M., Zhang, G., Zhang, S., Chen, Z., Chi, X., Dong, Y., Fan, P., Liu, Y., Chen, Y., Song, X., Liu, S., Yu, C., Li, J., & Xia, X. (2020). Characterization of two neutralizing antibodies against rift valley fever virus Gn protein. *Viruses*, *12*(3), 259. https://doi.org/10.3390/v12030259

Harmon, B., Schudel, B. R., Maar, D., Kozina, C., Ikegami, T., Tseng, C.-T. K., & Negrete, O. A. (2012). Rift Valley fever virus strain MP-12 enters mammalian host cells via caveola-mediated endocytosis. *Journal of Virology*, *86*(23), 12954–12970. https://doi.org/10.1128/JVI.02242-12

Huiskonen, J. T., Overby, A. K., Weber, F., & Grünewald, K. (2009). Electron cryo-microscopy and single-particle averaging of Rift Valley fever virus: evidence for GN-GC glycoprotein heterodimers. *Journal of Virology*, *83*(8), 3762–3769. https://doi.org/10.1128/JVI.02483-08

Ikegami, T., Won, S., Peters, C. J., & Makino, S. (2005). Rift Valley fever virus NSs mRNA is transcribed from an incoming anti-viral-sense S RNA segment. *Journal of Virology*, *79*(18), 12106–12111. https://doi.org/10.1128/JVI.79.18.12106-12111.2005

Kortekaas, J. (2014). One Health approach to Rift Valley fever vaccine development. *Antiviral Research*, *106*(June 2014), 24–32. https://doi.org/10.1016/J.ANTIVIRAL.2014.03.008

Li, Y. T., Wang, C. L., Zheng, X. X., Wang, H. L., Zhao, Y. K., Gai, W. W., Jin, H. L., Gao, Y. W., Li, N., Yang, S. T., & Xia, X. Z. (2016). Development and characterization of rift valley fever virus-like particles. *Genetics and Molecular Research*, *15*(1), gmr7772. https://doi.org/10.4238/gmr.15017772

Lozach, P. Y., Kühbacher, A., Meier, R., Mancini, R., Bitto, D., Bouloy, M., & Helenius, A. (2011). DC-SIGN as a receptor for phleboviruses. *Cell Host and Microbe*, *10*(1), 75–88. https://doi.org/10.1016/j.chom.2011.06.007

Mandell, R. B., Koukuntla, R., Mogler, L. J. K., Carzoli, A. K., Freiberg, A. N., Holbrook, M. R., Martin, B. K., Staplin, W. R., Vahanian, N. N., Link, C. J., & Flick, R. (2010a). A replication-incompetent Rift Valley fever vaccine: Chimeric virus-like particles protect mice and rats against lethal challenge. *Virology*, *397*(1), 187–198. https://doi.org/10.1016/J.VIROL.2009.11.001

Mandell, R. B., Koukuntla, R., Mogler, L. J. K., Carzoli, A. K., Holbrook, M. R., Martin, B. K., Vahanian, N., Link, C. J., & Flick, R. (2010b). Novel suspension cell-based vaccine production systems for Rift Valley fever virus-like particles. *Journal of Virological Methods*, *169*(2), 259–268. https://doi.org/10.1016/J.JVIROMET.2010.07.015

Murtey, M. Das. (2016). Immunogold Techniques in Electron Microscopy. In *Modern Electron Microscopy in Physical and Life Sciences* (pp. 143-160). InTech. https://doi.org/10.5772/61719

Näslund, J., Lagerqvist, N., Habjan, M., Lundkvist, Å., Evander, M., Ahlm, C., Weber, F., & Bucht, G. (2009). Vaccination with virus-like particles protects mice from lethal infection of Rift Valley Fever Virus. *Virology*, *385*(2), 409–415. https://doi.org/10.1016/J.VIROL.2008.12.012

Paweska, J. T., & Jansen van Vuren, P. (2013). Rift Valley Fever Virus: A Virus with Potential for Global Emergence. In *The Role of Animals in Emerging Viral Diseases* (pp. 169–200). Elsevier Inc. https://doi.org/10.1016/B978-0-12-405191-1.00008-9

Pfeffer, S., & Mahamid, J. (2018). Unravelling molecular complexity in structural cell biology. *Current Opinion in Structural Biology*, *52*, 111–118. https://doi.org/10.1016/J.SBI.2018.08.009

Piper, M. E., Sorenson, D. R., & Gerrard, S. R. (2011). Efficient Cellular Release of Rift Valley Fever Virus Requires Genomic RNA. *PLoS ONE*, *6*(3), e18070. https://doi.org/10.1371/journal.pone.0018070

Reddington, S. C., & Howarth, M. (2015). Secrets of a covalent interaction for biomaterials and biotechnology: SpyTag and SpyCatcher. *Current Opinion in Chemical Biology*, *29*, 94–99. https://doi.org/10.1016/J.CBPA.2015.10.002

Reiter, K., Aguilar, P. P., Wetter, V., Steppert, P., Tover, A., & Jungbauer, A. (2019). Separation of virus-like particles and extracellular vesicles by flow-through and heparin affinity chromatography. *Journal of Chromatography A*, *1588*, 77–84. https://doi.org/10.1016/J.CHROMA.2018.12.035

Renner, T., Bélanger, K., & Langlois, M.-A. (2018). Selective Isolation of Retroviruses from Extracellular Vesicles by Intact Virion Immunoprecipitation. *BIO-PROTOCOL*, *8*(17). https://doi.org/10.21769/BioProtoc.3005

SIB Swiss Institute of Bioinformatics: ViralZone (n. d.) Phlebovirus. Retrieved April 30, 2020, from https://viralzone.expasy.org/252

Sherman, M. B., Trujillo, J., Leahy, I., Razmus, D., DeHate, R., Lorcheim, P., Czarneski, M. A., Zimmerman, D., Newton, J. T. A. M., Haddow, A. D., & Weaver, S. C. (2013). Construction and organization of a BSL-3 cryo-electron microscopy laboratory at UTMB. *Journal of Structural Biology*, *181*(3), 223–233. https://doi.org/10.1016/j.jsb.2012.12.007

Spiegel, M., Plegge, T., & Pöhlmann, S. (2016). The Role of Phlebovirus Glycoproteins in Viral Entry, Assembly and Release. *Viruses*, *8*(7), 202. https://doi.org/10.3390/v8070202

Stark, H., & Chari, A. (2016). Sample preparation of biological macromolecular assemblies for the determination of high-resolution structures by cryo-electron microscopy. *Microscopy*, *65*(1), 23–34. https://doi.org/10.1093/jmicro/dfv367

Stass, R., Ilca, S. L., & Huiskonen, J. T. (2018). Beyond structures of highly symmetric purified viral capsids by cryo-EM. *Current Opinion in Structural Biology*, *52*, 25–31. https://doi.org/10.1016/J.SBI.2018.07.011

Steppert, P., Burgstaller, D., Klausberger, M., Tover, A., Berger, E., & Jungbauer, A. (2017).

Quantification and characterization of virus-like particles by size-exclusion chromatography and nanoparticle tracking analysis. *Journal of Chromatography A*, *1487*, 89–99. https://doi.org/10.1016/j.chroma.2016.12.085

van Niel, G., D'Angelo, G., & Raposo, G. (2018). Shedding light on the cell biology of extracellular vesicles. *Nature Reviews Molecular Cell Biology*, *19*(4), 213–228. https://doi.org/10.1038/nrm.2017.125

Wang, Q., Ma, T., Wu, Y., Chen, Z., Zeng, H., Tong, Z., Gao, F., Qi, J., Zhao, Z., Chai, Y., Yang, H., Wong, G., Bi, Y., Wu, L., Shi, R., Yang, M., Song, J., Jiang, H., An, Z., … Yan, J. (2019). Neutralization mechanism of human monoclonal antibodies against Rift Valley fever virus. *Nature Microbiology*, *4*(7), 1231–1241. https://doi.org/10.1038/s41564-019-0411-z

World Health Organization (2018). Rift Valley Fever [Fact Sheet]. Retrieved April 30, 2020, from https://www.who.int/news-room/fact-sheets/detail/rift-valley-fever

Wright, D., Kortekaas, J., Bowden, T. A., & Warimwe, G. M. (2019). Rift Valley fever: biology and epidemiology. *Journal of General Virology*, *100*(8), 1187–1199. https://doi.org/10.1099/jgv.0.001296

Yu, G., Li, K., Huang, P., Jiang, X., & Jiang, W. (2016). Antibody-Based Affinity Cryoelectron Microscopy at 2.6-Å Resolution. *Structure*, *24*(11), 1984–1990. https://doi.org/10.1016/J.STR.2016.09.008

Zeltins, A. (2013). Construction and Characterization of Virus-Like Particles: A Review. *Molecular Biotechnology*, *53*(1), 92–107. https://doi.org/10.1007/s12033-012-9598-4

9 SUPPORTING DATA

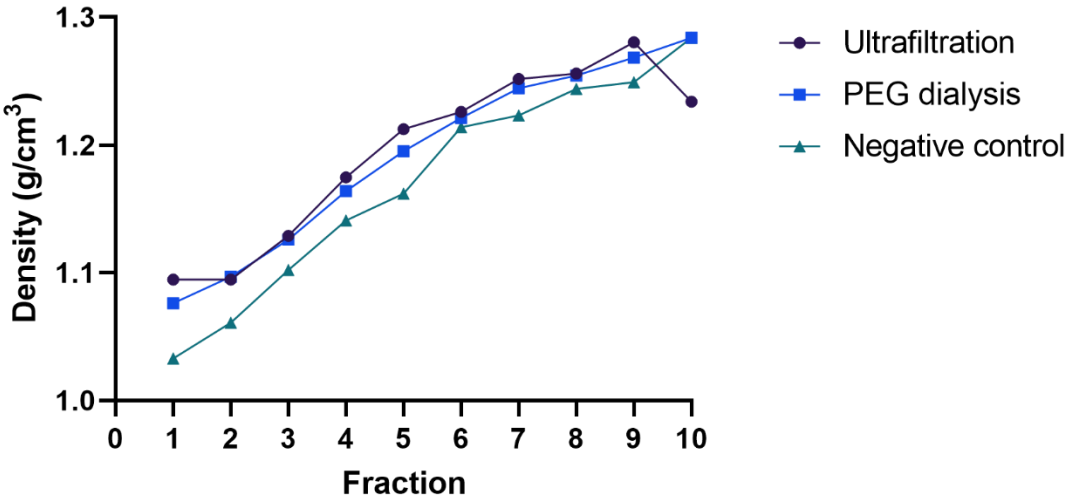

Figure S1. Density gradient graph plotted from density measurements. *Three samples fractionated: a non-transfected negative control, and transfected samples concentrated by ultrafiltration or PEG dialysis. The density of each fraction is plotted in the y-axis and the fraction numbers in the x-axis. The gradients display some irregularities but are roughly linear.*

Table S1. Formulation of LB medium.

10 g	Tryptone	HISPANLAB H1612
5 g	Yeast extract	HISPANLAB H1702
5 g	NaCl	RIEDEL 31434
ad. 1000 ml MilliQ H2O		

Table S2. Formulation of LB-agar.

9 g	Tryptone	HISPANLAB H1612
4.5 g	Yeast extract	HISPANLAB H1702
13.5 g	Agar	HISPANLAB H1800
4.5 g	NaCl	RIEDEL 31434
ad. 900 ml MilliQ H2O		

Table S3. Formulation of DMEM pH 7,4 (Dulbecco's modified eagle's medium).

135 g	Dulbecco's Modified Eagle's Medium - high glucose	SIGMA D-7777 (10 l)
37 g	$NaHCO_3$	(J.T.BAKER 0263)
Dissolved in 10 L sterile water, pH adjusted to 7.5 with 5 M HCl.		

Table S4. Formulation of Trypsin-EDTA pH 7,4.

1,25 g	Trypsin 1:250	DIFCO 0152-15
0,5 g	EDTA	J.T.BAKER 1073
20 g	NaCl	RIEDEL 31434
1 g	KCl	RIEDEL 31248
0,875 g	$NaHCO_3$	J.T.BAKER 0263
2,5 g	Glucose	ICN 194672
0,013 g	Phenol red	MERCK 7241
Dissolved in 2500 ml sterile water in total; pH adjusted to 7.4 with 5 M NaOH.		

Table S5. Centrifugation parameters for ultrafiltration procedures.

Filter capacity	Centrifugation speed	Centrifugation temperature	Initial sample volume range	Total centrifugation time for concentration
15 ml	3220 × g	+14°C	20-25 ml	30-40 min
4 ml	3220 × g	+14°C	10 ml	35 min
2 ml	3500 × g	~+20°C	0.1-0.4 ml	30 min
0.5 ml	14 000 × g	~+20°C	0.1-2 ml	15-30 min